Isovector Quadrupole Resonance Observed in the ^{60}Ni(^{13}C, ^{13}N)^{60}Co Reaction at $E/A = 100$ MeV

T. Ichihara,[1,*] M. Ishihara,[1] H. Ohnuma,[2] T. Niizeki,[3] Y. Satou,[4] H. Okamura,[5] S. Kubono,[4] M. H. Tanaka,[6] and Y. Fuchi[6]

[1]*RIKEN, 2-1 Hirosawa, Wako, Saitama 351-0198, Japan*
[2]*Department of Physics, Chiba Institute of Technology, Chiba 275-0023, Japan*
[3]*Faculty of Home Economics, Tokyo Kasei University, Tokyo 173-8602, Japan*
[4]*Center for Nuclear Study (CNS), University of Tokyo, Wako Branch at RIKEN, 2-1 Hirosawa, Wako, Saitama 351-0198, Japan*
[5]*Department of Physics, Saitama University, Saitama 338-8570, Japan*
[6]*High Energy Accelerator Research Organization (KEK), Tsukuba 305-0801, Japan*

(Received 10 June 2002; published 11 September 2002)

The charge-exchange reaction ^{60}Ni(^{13}C, ^{13}N)^{60}Co at $E/A = 100$ MeV has been studied to locate isovector ($\Delta T = 1$) non-spin-flip ($\Delta S = 0$) giant resonances. Besides the giant dipole resonance at $E_x = 8.7$ MeV, another resonance has been observed at $E_x = 20$ MeV with a width of 9 MeV. Distorted-wave Born approximation analysis on the angular distribution clearly indicated the $L = 2$ multipolarity, attributing the $E_x = 20$ MeV state to the giant isovector quadrupole resonance.

DOI: 10.1103/PhysRevLett.89.142501 PACS numbers: 24.30.Cz, 25.70.Bc, 25.70.Kk, 27.50.+e

Giant resonances represent major modes of collective motion, which dictate the dynamical properties of nuclei. For a nucleus as a many-body system of nucleons, various multipole modes exist reflecting isospin (T) and spin (S) degrees of freedom. The isoscalar ($\Delta T = 0$) and isovector ($\Delta T = 1$) modes represent oscillations in which protons and neutrons move in phase and in opposite phase, respectively, while electric ($\Delta S = 0$) and magnetic ($\Delta S = 1$) modes correspond to non-spin-flip and spin-flip excitations, respectively. Among the isovector non-spin-flip modes, the dipole resonance (IVGDR; $L = 1$) has been explored most extensively and is known to prevail over the nuclear chart. On the other hand, only limited information has been obtained so far for the monopole (IVGMR; $L = 0$) and quadrupole resonances (IVGQR; $L = 2$) [1].

These two modes are supposed to be coherent states of $1p$-$1h$ excitations across two major shells ($2\hbar\omega$), while the IVGDR is related to excitations of one major shell ($1\hbar\omega$). Accordingly the IVGMR and IVGQR are expected to appear at similar excitation energies, which are considerably higher than $82\ A^{-1/3}$ MeV expected for the IVGDR. At such higher energies, the excitation spectrum becomes progressively complex with mixed contributions from various excitation modes on top of the mounting continuum background. The broader width of the resonance further increases the difficulty for identification.

In recent years, several attempts have been made to locate these high-lying resonances by employing charge-exchange reactions. Among those studies, measurements with reactions of (π^-, π^0) at 165 MeV [2], (^{7}Li, ^{7}Be) at $E/A = 65$ MeV [3], and (^{3}He, tp) at $E/A = 59$ MeV [4] provided strong indications for the existence of the IVGMR. On the other hand, clear observation of an IVGQR has been so far unsuccessful, while its occurrence was suggested from the forward-backward asymmetry due to the E1-E2 interference in (γ, n) and (n, γ) reactions [5], and by the multipole decomposition analysis of the inelastic electron scattering [6].

In this Letter we report on the first clear identification of the IVGQR in the ^{60}Ni(^{13}C, ^{13}N)^{60}Co reaction at $E/A = 100$ MeV. For comparison, a measurement on the (^{12}C, ^{12}N) reaction was also performed. These heavy ion reactions afford several advantages in probing the giant resonances of interest. First of all, they exhibit strong selectivity for $\Delta T = 1$ and $\Delta T_z = 1$ excitations, uniquely populating the isovector $T + 1$ resonances. As for the spin selectivity, the (^{13}C, ^{13}N) reaction allows $\Delta S = 0, 1$ excitations while the (^{12}C, ^{12}N) reaction allows only $\Delta S = 1$ excitations. For the former reaction, it is also known that $\Delta S = 0$ components are much more favored than $\Delta S = 1$ components because of its large Fermi matrix element ($M_F/M_{GT} \sim 5$) [7]. Hence the combination of these two reactions could provide a useful means to distinguish between spin-flip and non-spin-flip modes.

There exist earlier measurements on the (^{13}C, ^{13}N) reaction performed at $E/A = 50$–60 MeV [7,8]. However, the observed angular distributions turned out to be rather structureless, disallowing L determination for the resonances. This is thought to be due to considerable contributions of multistep processes at these energies. In contrast, it has been shown for the (^{12}C, ^{12}N) reaction that such contributions become almost negligible in the higher-energy domain of $E/A \geq 100$ MeV [9,10]. Given all these favorable features, the high-energy (^{13}C, ^{13}N) reaction can be expected to make a powerful tool to locate the $\Delta S = 0$ and $\Delta T = 1$ resonances.

The measurements were performed using $E/A = 100$ MeV ^{13}C and $E/A = 135$ MeV ^{12}C beams from the K540 RIKEN Ring Cyclotron and the spectrograph

SMART [11] with QQDQD (Q: quadrupole; D: dipole) configuration. The elastic scattering was also measured for the ^{13}C beam. A self-supporting enriched ^{60}Ni target of 3.0 mg/cm^2 was used, resulting in an overall energy resolution of 1 MeV. The spectrograph had a large angular acceptance of 200 mr for vertical and 50 mr for horizontal planes. The spectrograph was equipped with a pair of cathode readout drift chambers (CRDC) [12] at the focal plane. Plastic scintillation counters placed behind the CRDC's provided ΔE and time of flight signals for particle identification. The momentum as well as the vertical and horizontal scattering angles was obtained by reconstructing the trajectory through the two CRDC's. The overall angular resolution achieved was estimated to be approximately 0.1°. Thus differential cross sections were obtained for every 0.2° bin of the scattering angle (lab.) for the charge-exchange reactions.

Figure 1 shows typical energy spectra of the ^{60}Ni(^{13}C, ^{13}N)^{60}Co reaction at $E/A = 100$ MeV. Data at two angular bins, $\theta_{\rm lab} = 0°$–$0.2°$ and $\theta_{\rm lab} = 0.8°$–$1.0°$, are shown together with the difference spectrum between these two bins. The excitation energies are given with respect to the ground state of ^{60}Co. The difference spectrum is also shown for the ^{60}Ni(^{12}C, ^{12}N)^{60}Co reaction at $E/A = 135$ MeV for the sake of comparison. The peak from the ^{1}H(^{13}C, ^{13}N)n is seen at the low excitation energies. The other contributions from the target contamination are estimated to be negligible.

The energy spectra are dominated by resonance structures built on top of a large continuum background. The profiles of resonances are most clearly indicated in the difference spectra: The difference spectrum for ^{60}Ni(^{13}C, ^{13}N)^{60}Co shows two resonances at $E_x = 8.7$ and 20 MeV, while that for ^{60}Ni(^{12}C, ^{12}N)^{60}Co shows a resonance at $E_x = 10$ MeV. The difference of the resonance structure between the two reactions can be attributed to the ΔS selectivity. In the (^{12}C, ^{12}N) reaction only $\Delta S = 1$ states will be excited. Hence the resonance at $E_x = 10$ MeV can be assigned to a $\Delta S = 1$ resonance consistently with Refs. [3,13]. On the other hand, the (^{13}C, ^{13}N) reaction favors $\Delta S = 0$ excitations over $\Delta S = 1$ excitations [7]. Thus the two resonances at $E_x = 8.7$ and 20 MeV may be assigned to be $\Delta S = 0$ states. The absence of these peaks in the (^{12}C, ^{12}N) spectrum supports this conclusion.

In order to extract yields of the observed resonances, subtraction of the continuum background is crucial. The origin of the background may be mainly attributed to the quasi-free charge-exchange reactions. We used the functional form of Erell *et al.* [2] to express the double differential cross sections for the continuum background. This expression has four parameters, central ejectile energy $E_{\rm QF}$, its width W_L, maximum cutoff energy E_0, and a cutoff energy scale parameter T. We have assumed $E_{\rm QF} = E_{\rm free} - S_n$, where $E_{\rm free}$ is the energy of ^{13}N for the p(^{13}C, ^{13}N)n reaction and S_n is the neutron separation energy of ^{60}Co. The parameter E_0 was set at 0 MeV to accommodate the contributions from unresolved discrete levels as well as three-body continuum states.

Peak fitting procedure has been performed for the 20 spectra of the ^{60}Ni(^{13}C, ^{13}N)^{60}Co reaction over the angular range from $\theta_{\rm lab} = 0°$–$0.2°$ bin to $\theta_{\rm lab} = 3.8°$–$4.0°$ bin. Peak shapes for $E_x = 8.7$ MeV and $E_x = 20$ MeV states were assumed to be Gaussian. The value of T was set to be same for the entire angular range while the angular dependence was introduced for W_L. After a systematic search we found that the parameter set of $W_L = 34(1.0 + 0.06\theta_{\rm lab} + 0.06\theta_{\rm lab}^2)$ MeV and $T = 15.5$ MeV reproduces the continuum background consistently for all the angles involved ($\chi^2/f = 1.5$).

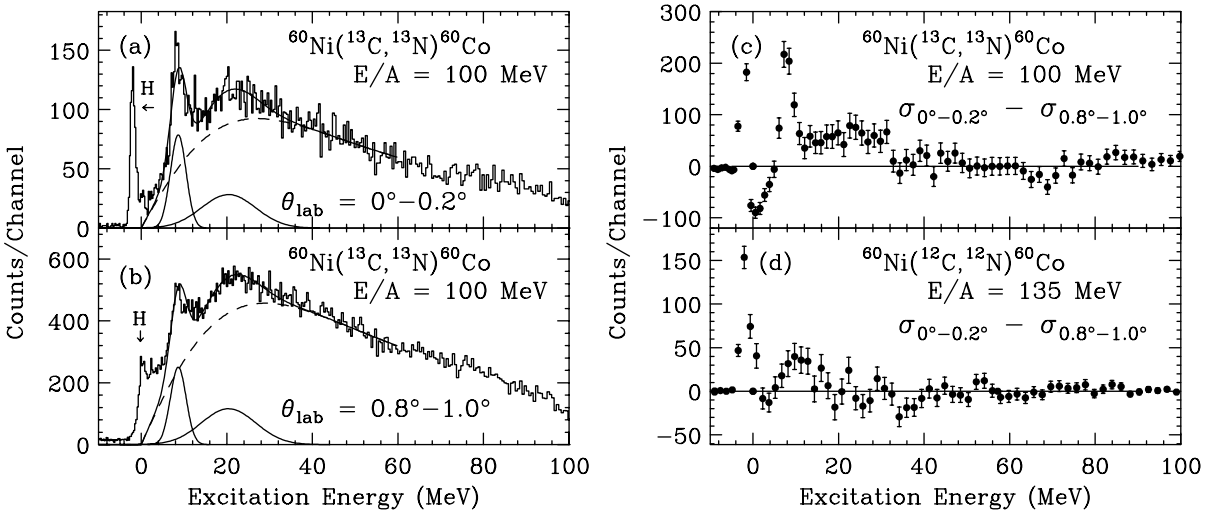

FIG. 1. Energy spectra of the ^{60}Ni(^{13}C, ^{13}N)^{60}Co reaction for the angular bins of (a) $\theta_{\rm lab} = 0°$–$0.2°$ and (b) $\theta_{\rm lab} = 0.8°$–$1.0°$. The symbol H refers to the ^{1}H(^{13}C, ^{13}N)n reaction. (c) represents the difference spectrum obtained by subtracting (b) from (a) after renormalization. (d) represents the difference spectrum obtained for the ^{60}Ni(^{12}C, ^{12}N)^{60}Co reaction.

TABLE I. Excitation energies and widths of the resonances observed in $\Delta T_z = 1$ charge-exchange reactions leading to ^{60}Co.

	$(1\hbar\omega)$		$(2\hbar\omega)$		Ref.
	E_x (MeV)	Γ (MeV)	E_x (MeV)	Γ (MeV)	
(π^-, π^0)	10.7 ± 1.6	4.2 ± 2.0	22.4 ± 1.7	14.7 ± 2.1	[2]
(^{7}Li, ^{7}Be)	8.5 ± 0.5	4.0 ± 0.5	20 ± 2	10 ± 2	[3]
(^{13}C, ^{13}N)	9.1 ± 0.3	2.2 ± 0.4	22.1 ± 0.8	8.1 ± 1.0	[7]
Present work	8.7 ± 0.5	2.8 ± 0.8	20 ± 2	9 ± 2	

Typical results from the fitting procedure are found in Fig. 1. The dashed curves show the calculated continuum spectra, which well reproduce the overall feature of the background. The solid curves in Fig. 1, obtained by superposing the two Gaussian peaks of the resonances, reproduce the experimental data very well. The energy and width (Γ) of the two resonances thus determined are listed in Table I together with the previous results on various (n, p)-type exchange reactions on ^{60}Ni. All the measurements exhibited two prominent peaks at about 9 and 20 MeV. The assignment of the IVGDR to the lower-energy peak is consistently supported. On the other hand, there exist different possibilities for the higher-energy peak. While the works on the (π^-, π^0) [2] and (^{7}Li, ^{7}Be) [3] reactions claimed the $L = 0$ assignment, the work on the (^{13}C, ^{13}N) reaction at $E/A = 50$–60 MeV [7,8] was unable to confirm the $L = 0$ nature of the resonance. A recent self-consistent random phase approximation calculation indicates that the IVGQR strength of ^{60}Co is peaked around 23 MeV and that of the IVGMR around 26 MeV [14]. It is thus plausible that the IVGQR as well as the IVGMR gives rise to a high-energy peak.

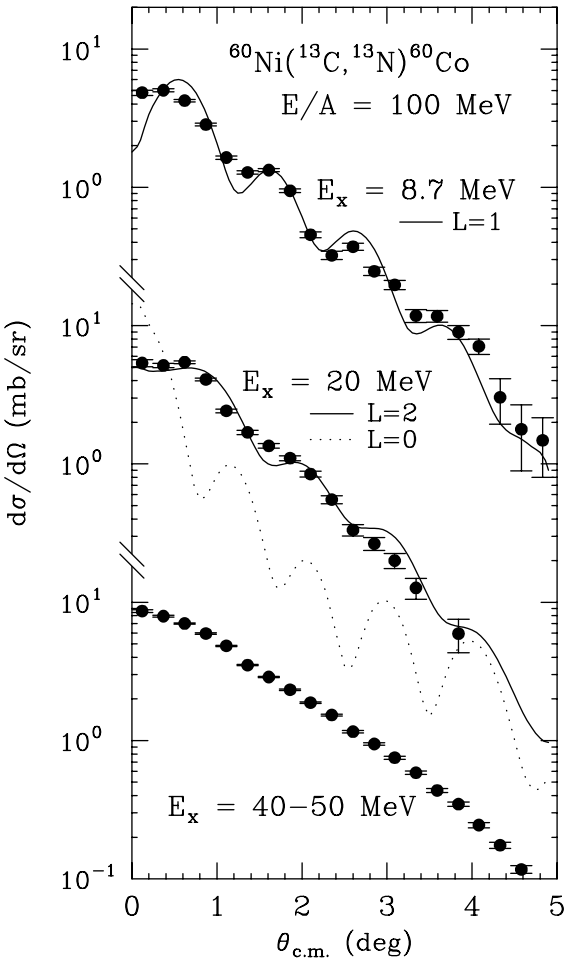

FIG. 2. Differential cross sections for the $E_x = 8.7$ MeV and $E_x = 20$ MeV states and the background sum of $E_x =$ 40–50 MeV of the ^{60}Ni(^{13}C, ^{13}N)^{60}Co reaction at $E/A =$ 100 MeV. Error bars represent only statistical ones. Curves are obtained from DWBA calculations as described in the text.

The extracted angular distributions for $E_x = 8.7$ MeV and $E_x = 20$ MeV states are plotted in Fig. 2. They exhibit clear diffraction patterns, suggesting dominance of the one-step process at $E/A = 100$ MeV. In order to determine the multipolarity (L) of the resonances, microscopic distorted-wave Born approximation (DWBA) calculations were performed using the code developed by Lenske [15]. Optical-potential parameters were determined by fitting the present data on the ^{60}Ni(^{13}C, ^{13}C)^{60}Ni elastic scattering with the code ECIS79 [16]. They are summarized in Table II, and the calculated angular distribution is compared with the experiment in Fig. 3. In the DWBA calculations, the form factors of $L = 0$, 1, and 2 were obtained by folding the transition densities of the projectile and the target with the effective interaction [17]. The transition density of the projectile was obtained from the shell-model single-particle wave functions [9], while the transition density of the target was assumed to take a collective form of the Tassie type [1,18] with Wood-Saxon radial distribution of $r_0 = 1.2$ fm and $a = 0.6$ fm.

The solid curves in Fig. 2 represent the results of the DWBA calculations. They are obtained after folding the

TABLE II. Optical-potential parameters deduced from the ^{60}Ni(^{13}C, ^{13}C)^{60}Ni reaction at $E/A = 100$ MeV.

V_r (MeV)	r (fm)	a (fm)	W_r (MeV)	r_w (fm)	a_w (fm)
52.8	1.09	0.79	35.0	0.87	1.78

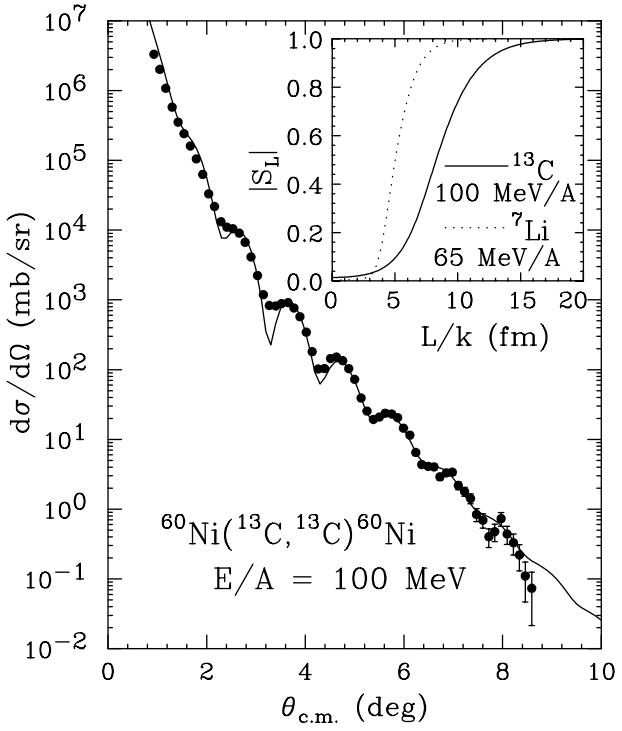

FIG. 3. Differential cross sections for the elastic scattering of ^{13}C from ^{60}Ni. The solid curve is calculated with the parameters in Table II and folded with the experimental angular resolution. The inset shows the absolute values of the S-matrix elements (S_L) calculated for the ^{60}Ni(^{13}C, ^{13}C)^{60}Ni reaction at $E/A = 100$ MeV and ^{60}Ni(^{7}Li, ^{7}Li)^{60}Ni reaction at $E/A = 65$ MeV (Ref. [3]). The horizontal axis is the orbital angular momentum (L) divided by the wave number (k).

calculated results with experimental angular resolutions and by normalizing the absolute magnitudes to the experimental data. For the $E_x = 8.7$ MeV state, an IVGDR was assumed. Hence the $L = 1$ form factor was taken. Indeed, a very good fit has been obtained, justifying the validity of the DWBA analysis. For the $E_x = 20$ MeV state, we have studied two cases, one with the $L = 0$ IVGMR form factor and the other with the $L = 2$ IVGQR form factor. The calculated angular distribution for the $L = 0$ IVGMR (the dotted curve in Fig. 2) exhibits a steep rise at 0° and the first minimum near the $\theta_{cm} = 0.8°$. However, these distinctive features are hardly manifested in the observed angular distribution. On the other hand, an excellent fit has been obtained with the calculated distribution for the $L = 2$ IVGQR excitation. This result strongly indicates that the resonance state observed at $E_x = 20$ MeV is an IVGQR rather than an IVGMR. The present DWBA analysis further indicates that the observed peak exhausts approximately 50% strength of the isovector $L = 2$ classical energy-weighted sum rule [19].

The present observation of the IVGQR raises a puzzling problem why the (^{13}C, ^{13}N) reaction favorably excites the IVGQR while other reactions such as (^{7}Li, ^{7}Be) reportedly populate only the IVGMR. In this respect, we have examined the radial overlap of the form factor with the penetrability profile of the probe particles. The inset of Fig. 3 shows a comparison of the penetrability profiles of the present (^{13}C, ^{13}N) reaction at $E/A = 100$ MeV and (^{7}Li, ^{7}Be) at $E/A = 65$ MeV [3] obtained by using the optical potentials as employed in the relevant analyses. It was found that the former reaction is much more peripheral than the latter. On the other hand, the form factor for the IVGMR is mostly distributed in the interior of the nucleus while that for the IVGQR is shifted towards the surface region. Hence it is plausible that the excitation of the IVGQR is favored in the (^{13}C, ^{13}N) reaction while that of the IVGMR is favored in the (^{7}Li, ^{7}Be) reaction.

In summary, we have studied the ^{60}Ni(^{13}C, ^{13}N)^{60}Co reaction at $E/A = 100$ MeV to observe isovector non-spin-flip giant resonances. Besides the IVGDR at $E_x = 8.7$ MeV, a significant peak was observed at $E_x = 20$ MeV with a width of 9 MeV. DWBA analysis of the observed angular distribution clearly indicates $L = 2$ multipolarity, revealing the occurrence of the IVGQR. No evidence of the IVGMR was observed by the present experiment.

We are grateful to Dr. I. Hamamoto and Dr. H. Sagawa for their stimulating discussions.

*Electronic address: ichihara@riken.go.jp

[1] M. N. Harakeh and A. van der Woude, *Giant Resonances* (Oxford University Press, New York, 2001).
[2] A. Erell *et al.*, Phys. Rev. C **34**, 1822 (1986).
[3] S. Nakayama *et al.*, Phys. Rev. Lett. **83**, 690 (1999).
[4] R. G. T. Zegers *et al.*, Phys. Rev. Lett. **84**, 3779 (2000); Phys. Rev. C **63**, 034613 (2001).
[5] D. A. Sims *et al.*, Phys. Rev. C **55**, 1288 (1997).
[6] Y. Torizuka *et al.*, Phys. Rev. C **11**, 1174 (1975).
[7] C. Bérat *et al.*, Nucl. Phys. **A555**, 455 (1993).
[8] I. Lhenry *et al.*, Nucl. Phys. **A599**, 245c (1996).
[9] T. Ichihara *et al.*, Phys. Lett. B **323**, 278 (1994); Nucl. Phys. **A577**, 93c (1994); **A583**, 109c (1995).
[10] H. Lenske, H. H. Wolter, and H. G. Bohlen, Phys. Rev. Lett. **62**, 1457 (1989).
[11] T. Ichihara *et al.*, Nucl. Phys. **A569**, 287c (1994).
[12] M. H. Tanaka *et al.*, Nucl. Instrum. Methods Phys. Res., Sect. A **A362**, 521 (1995).
[13] A. L. Williams *et al.*, Phys. Rev. C **51**, 1144 (1995).
[14] G. Colò (private communication).
[15] H. Lenske, Nucl. Phys. **A482**, 343c (1988).
[16] J. Raynal, code ECIS79 (unpublished).
[17] M. A. Franey and W. G. Love, Phys. Rev. C **31**, 488 (1985).
[18] L. J. Tassie, Aust. J. Phys. **9**, 407 (1956).
[19] A. Bohr and B. R. Mottelson, *Nuclear Structure* (World Scientific, Singapore, 1998), Vol. 2, Eq. (6-177).